

# Suborganelle-Specific Protein Complex Analysis Enabled by in Vivo Cross-Linking Coupled with Proximal Labeling

Yuxin An, Qun Zhao,\* Zhou Gong, Lili Zhao, Yi Li, Zhen Liang, Peng Zou, Yukui Zhang, and Lihua Zhang\*



Cite This: *Anal. Chem.* 2022, 94, 12051–12059



Read Online

ACCESS |



Metrics & More

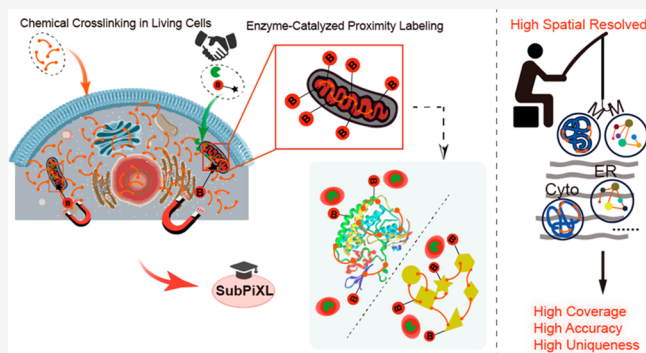


Article Recommendations



Supporting Information

**ABSTRACT:** The identification of the structure of protein complexes in the subcellular niche of cells is necessary to understand their diverse functions. In this study, we developed a suborganelle proteome labeling assisted in vivo cross-linking (SubPiXL) strategy to identify regional protein conformations and interactions in living cells. Due to the mitochondria's functional importance and well-defined compartmental partitions, the specific conformations and interactome of protein complexes located in the mitochondrial matrix were identified. Compared to the commonly used approach of organelle isolation followed by intact mitochondria cross-linking, our method achieved a more refined spatial characterization for the subcompartment of the cellular organelle. Additionally, this approach avoided cross-contamination and cell microenvironment disruption during organelle isolation. As such, we achieved 73% selectivity for mitochondria and 98% specificity of known suborganelle annotation for the mitochondrial matrix and accessible inner membrane. Meanwhile, more protein–protein interactions (PPIs) with high dynamics were captured, resulting in a 1.67-fold increase in the number of PPI identifications in 1/11th of the time. On the basis of these structural cross-links and the specific characterization of the interactome and conformation, the structural dynamics targeted in the mitochondrial matrix were delineated. Mitochondrial matrix-restricted information for proteins with multisubcellular localizations was then clarified. In summary, SubPiXL is a promising technique for the investigation of suborganelle-resolved protein conformation and interaction analysis and contributes to a better understanding of structure-derived functions.



## INTRODUCTION

Protein complexes are assembled and spatiotemporally organized in a sophisticated manner. In contrast to in vitro milieu, the interior of living cells consists of fine subcellular compartments with crowding and confinement effects.<sup>1</sup> The subcellular location of proteins is useful in the determination of protein function and can reveal the mechanism of molecular interactions. Different chemical environments exist in each subcellular organelle, such as biomolecular ligands, substrates, pH, and redox conditions.<sup>2,3</sup> These features provide the fundamental cellular basis for the specific assembly of protein complexes via conformational and interactional changes, allowing for the regulation of cell communication and substance exchange.<sup>4</sup> Therefore, an in-depth analysis of the protein complexes at a subcellular resolution is important for the identification of the structure and function of cells.

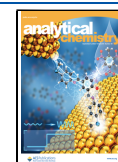
Affinity purification technology coupled with mass spectrometry (AP-MS) has been widely used to identify subnetworks of bait proteins and their interactors.<sup>5</sup> The combination of this with subcellular organelle isolation allowed us to obtain the protein–protein interactions (PPIs) of bait proteins associated within the

specific region.<sup>6</sup> Alternatively, chemical cross-linking combined with mass spectrometry (XLMS) has become a valuable technology used in proteome-wide profiling of the interaction interface and conformation of protein complexes.<sup>7</sup> Recent advancements in in vivo cross-linking have revealed protein conformation and interactions in their native environment by covalently linking the two amino acid residues in and between proteins within the constraints of cross-linking distance.<sup>8,9</sup> This approach is superior to AP-MS, identifies some weak/transient interactions, and determines direct PPIs. However, in existing in vivo cross-linking studies, only cross-linking of the whole cells is achieved. In this case, the regionally specific structure of the protein complex is obscured by homogenization of the whole cell, making specific analysis within the targeted region

**Received:** April 13, 2022

**Accepted:** August 18, 2022

**Published:** August 25, 2022



impossible. Moreover, due to the complexity of the cross-linked products and expanded search space, XLMS analysis of specific subcellular organelles suffers from poor sensitivity. In this case, organelle isolation followed by cross-linking of the intact nuclear or mitochondria was developed to facilitate spatial resolution. Nevertheless, we found that (i) most subcellular compartments are not amenable to genuine “purification” due to their intrinsic heterogeneity and overlapping physical properties; (ii) subcellular organelle isolation and *in vitro* environments change the structure and function of their internal proteins; (iii) further finer suborganelle-resolved analysis (such as mitochondrial matrix, nuclear lamina) is difficult to perform.<sup>10</sup>

Enzyme-catalyzed proximity labeling (PL) has been recently applied to a wide variety of subcellular compartments, such as the mitochondrial intermembrane space (IMS) and outer membrane (OMM), the endoplasmic reticulum (ER)–plasma membrane contact, and primary cilia, enabling selective tagging of specific subcellular organelle proteins and generating high-quality protein inventories for human cells, yeast, *Drosophila*, and other organisms.<sup>11,12</sup> PL technology has been used for interactional analysis by fusing it with subcellular markers to label and enrich proteins with a 10 nm radius of baits, along with SAINT express analysis to determine the probability of it being a true interaction.<sup>13</sup> However, due to the lack of interface sites and structural distance restraints, this approach cannot be used to analyze protein conformation and interaction docking.

In this study, we developed a SubPiXL (suborganelle proteome labeling assisted *in vivo* cross-linking) strategy by combining the *in vivo* cross-linking with PL to decipher the suborganelle-resolved conformation and interaction of protein complexes. When the functional importance of mitochondria and their well-defined structural partition were considered, the mitochondrial matrix (including the accessible inner membrane) was considered a proof of concept. The protein complexes located in the mitochondrial matrix were exclusively tagged by SubPiXL while being cross-linked, which allows for the selective enrichment and in-depth identification of the cross-linking information on the targets. On the basis of the advantages of targeting, accuracy, and SubPiXL coverage, the protein conformations and interactions in the mitochondrial matrix could be globally identified. Therefore, their specific structures in the mitochondrial matrix were clarified and distinguished from those of other cellular compartments.

## EXPERIMENTAL SECTION

**Reagents and Cell Culture.** HEK293T cell lines stably expressing mitochondrial targeted APEX2 (V5-mito-APEX2) were cultured in a Dulbecco's Modified Eagle's Medium (DMEM) supplemented with 10% fetal bovine serum (FBS), 100 units/mL penicillin, and 100 mg/mL streptomycin at 37 °C under 5% CO<sub>2</sub>.<sup>14</sup> Cell line construction is provided in detail in the [Supporting Methods](#).

**DSDHD Synthesis.** The *disuccinimidyl dihydroxydecaedioate* (DSDHD) synthesis route is shown in [Scheme S1](#), and the obtained DSDHD was characterized by NMR and LC-MS ([Figures S1 and S2](#)).

**APEX2 Labeling Coupled with *in Vivo* Cross-linking.** HEK293T cells stably expressing V5-mito-APEX2 were grown and plated on three poly-D-lysine-covered 10 cm dishes (3 × 10<sup>7</sup> cells in total). The cells were incubated with 5 mL of 500 mM biotin–phenol in media for 30 min at 37 °C and 5% CO<sub>2</sub>. H<sub>2</sub>O<sub>2</sub> was then added to a final concentration of 1 mM for 1 min at room temperature (RT) to initiate the biotinylation reaction.

The reaction was then quenched with “quencher solution” (10 mM sodium ascorbate, 10 mM sodium azide, and 5 mM Trolox in DPBS) for 2 min. Subsequently, cells were washed with 5 mL of DPBS (pH 7.4) once. The same volume of ready-made DSDHD with a final concentration of 5 mM (1% DMSO) in DPBS was then added to the cells, and rotation was continued for 5 min. After *in vivo* cross-linking, the supernatant was removed, and cells were collected with 1 mL of DPBS. 2 M NH<sub>4</sub>HCO<sub>3</sub> was added to the final concentration of 50 mM, and the cross-linking reaction was quenched for 5 min. Cross-linked cells were centrifuged and collected. The whole-cell cross-linking of HEK 293T cells with DSDHD was performed as described above.

**SubPiXL and Whole-Cell Cross-Linking Sample Preparation.** The cell pellet was thawed on ice and lysed in 1 mL of RIPA buffer with 10 mM sodium ascorbate, 10 mM sodium azide, 5 mM Trolox, 1× protease inhibitor cocktail, and 1 mM PMSF by gentle pipetting and combined with sonication for 2 min (5 s on/10 s off pulse). A 4-fold volume of cold acetone was adopted for overnight protein precipitation at –20 °C. The resulting protein pellet was then moved to a fresh tube, washed three times with cold acetone, and dried at RT. The protein pellet was then dissolved with 0.5% SDS (w/v). Next, the SDS concentration was reduced to 0.1% with DPBS, and 2.8 mg of protein determined by the BCA protein assay was used for further processing. Cell lysates of SubPiXL were incubated with 120 μL of prewashed streptavidin beads at room temperature for 2 h, and then, the beads were washed twice with 1% SDS, 8 M urea, and 2 M NaCl (PBS) to remove nonspecific absorption. Before on-bead digestion, proteins on the beads were incubated with 0.3 M urea and 10 mM DTT at RT for 1 h and alkylated with 20 mM iodoacetamide in the dark at RT for 30 min. Beads were washed twice with NH<sub>4</sub>HCO<sub>3</sub> to remove excess small molecules and treated with 600 ng of Lys-C and 2 μg of trypsin for 16 h at 37 °C. Thereafter, released peptides were collected from the supernatant.

**2D LC-MS/MS Analysis.** High pH reversed phase fractionation was performed, and each fraction was analyzed with an Easy-nano LC 1200 system coupled to an Orbitrap Exploris 480 instrument with a FAIMS Pro device (Thermo Fisher Scientific). The details of the 2D LC-MS/MS analysis procedures are in the [Supporting Methods](#). The mass spectrometry raw data have been deposited with the ProteomeXchange Consortium with the data set identifier PXD034768.

**Data Analysis.** All the raw files were first processed with pFind 3.0 against the Human Uniprot FASTA database (2019-04-04). Trypsin was set as the enzyme, and up to 3 missed cleavage sites were allowed. Carbamidomethyl (C) was chosen for the fixed modifications; oxidation on methionine, acetylation of the protein N-terminus, and dead-end modification of DSDHD (+244.131 on K) were set as variable modifications. Mass tolerance of MS1 and MS2 scans was set to 10 ppm, and peptides were filtered with the false discovery rate (FDR) of ≤1%. Then, all proteins containing more than two DSDHD modified peptides were used to create a database for cross-linked peptide searching. Cross-link identification was performed using pLink 2.3.9 against the corresponding database with the following settings: MS and MS2 tolerance of 10 ppm, peptide mass of 500–6000, enzyme trypsin with up to 3 missed cleavages, cross-linker DSDHD (cross-linking sites K and protein N terminus, cross-link mass shift of 226.120, monolink mass shift of 244.131), fixed modification carbamidomethyl[C],

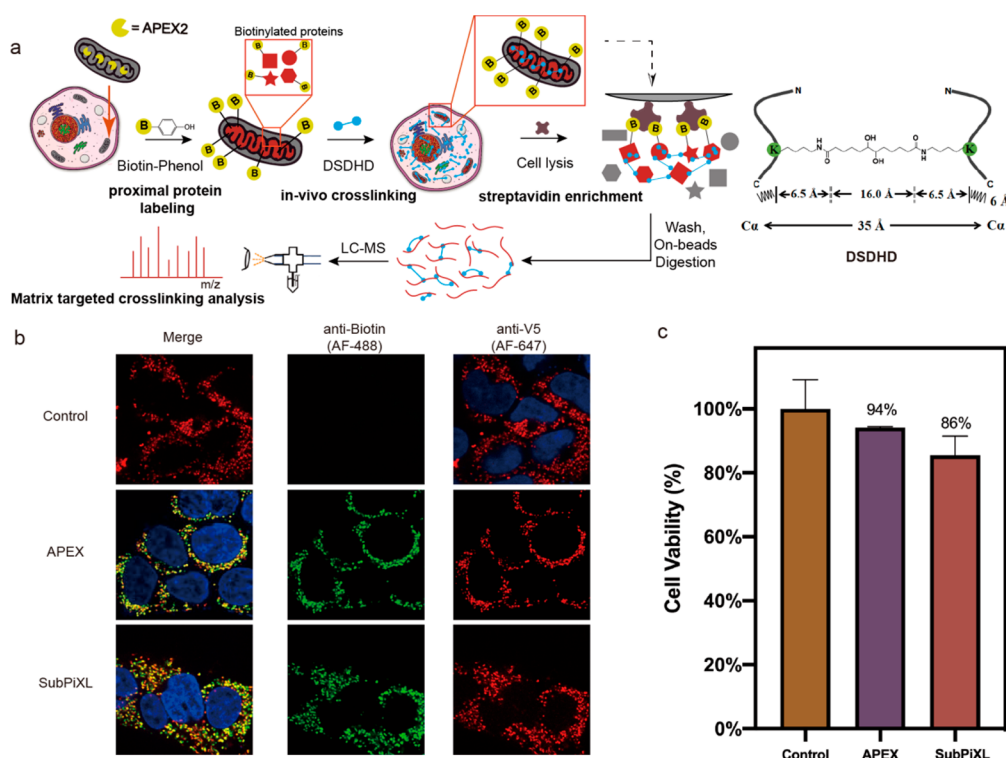


**Figure 1.** Establishment and evaluation of the SubPiXL strategy. (a) Schematic illustration of SubPiXL strategy. The APEX peroxidase was genetically targeted to the mitochondrial matrix. B represents biotin. (b) Confocal immunofluorescence imaging of biotinylated proteins. The control was performed with  $\text{H}_2\text{O}_2$  omitted. The cells were fixed and stained with anti-V5 to detect mito-APEX2 (AF647) and anti-biotin to detect the APEX2 labeling signal (AF488). Cell nuclei were stained with DAPI (blue). (c) Viability determination via CCK-8 assay analysis for cells treated by APEX and SubPiXL as well as the negative control of the untreated cells.

variable modification acetyl[Protein N-term], and oxidation-[M]. To filter for high-confidence data, an FDR of 1% on peptide spectra match (PSM) level was applied.

**Structure Validation, Protein Modeling, and Protein–Protein Interaction Docking.** The molecular dynamics option of Chem3D 19.0 with standard settings (step interval = 2.0 fs, frame interval = 10 fs, terminate after = 10 000 steps, heating/cooling rate = 1.000 kcal/atom/ps, and target temperature = 300 K) was used for the DSDHD arm length calculation, which is 16 Å. In addition to two lysine side chain lengths of 13 Å and a typical tolerance of 6 Å according to ref 15, lysine residues with a  $\text{C}\alpha$ – $\text{C}\alpha$  distance of <35.0 Å were expected to be preferentially cross-linked. Related  $\text{C}\alpha$ – $\text{C}\alpha$  euclidean straight-line distances (SLDs) were visualized with the PyMol Molecular Graphics System, version 2.0 Schrödinger; the solvent accessible surface distance (SASD) of the corresponding structures was calculated using TopoLink<sup>16</sup> (build 19.156). For ATP synthase and the HSPD1–HSPE1 complex, which contains large numbers of homologous proteins, the identified cross-links could come from within or between different subunits. To better present the protein structure with these cross-links, we used the shortest distance possible for all theories. Ensemble refinement against the cross-linking restraints was performed using Xplor-NIH. Detailed cross-link information is displayed in Tables S1–S4. Structures with no violation of cross-linking restraints and no clashed residues were used for further structural analysis. We performed the calculation 240 times for each analysis.

## RESULTS AND DISCUSSION

**Establishment of the SubPiXL Strategy.** To identify the components, conformation, and interactions of suborganelle-

specific proteomes, a universal SubPiXL strategy was developed in this work. We chose to work on the APEX2 due to its rapid and efficient proximity-dependent biotinylation in 1 min, coupled with fast cross-linking in living cells for 5 min<sup>17,18</sup> to covalently link the lysine within or between subunits of the protein complex. A snapshot of the dynamic structure of all proteins under their native environment was provided, while protein complexes located in the subcellular compartments were exclusively biotinylated and can be selectively isolated by affinity purification with streptavidin agarose. Along with on-bead digestion and LC-MS analysis, the proteome-wide components, structures, and interaction information within the targeted suborganelle were identified. Considering the well-defined compartments in the mitochondria, which cannot be analyzed using other biochemical fractionation methods, the SubPiXL strategy was applied to the mitochondrial matrix to decipher the region-restricted protein conformations and interactions and to clarify their differences from other intracellular locations (Figure 1a). This has allowed us to extend in situ cross-linking from the widely studied whole-cell level to focus on the subcellular organelle level.

To achieve fast cross-linking of the protein complex of living cells, a flexible homobifunctional *N*-hydroxysuccinimidyl (NHS) ester cross-linker of DSDHD was designed (Scheme S1, Figures S1 and S2) with proper amphipathy (Figure S3). The long alkyl chain provides the lipophilicity and a wider reaction radius, while the *o*-hydroxy group was introduced to increase its water solubility. Previous work has shown that this trifunctional cross-linker BSP can achieve in-depth in vivo cross-linking in minutes,<sup>18</sup> therefore, we performed a head-to-head comparison with BSP to characterize the in vivo cross-linking

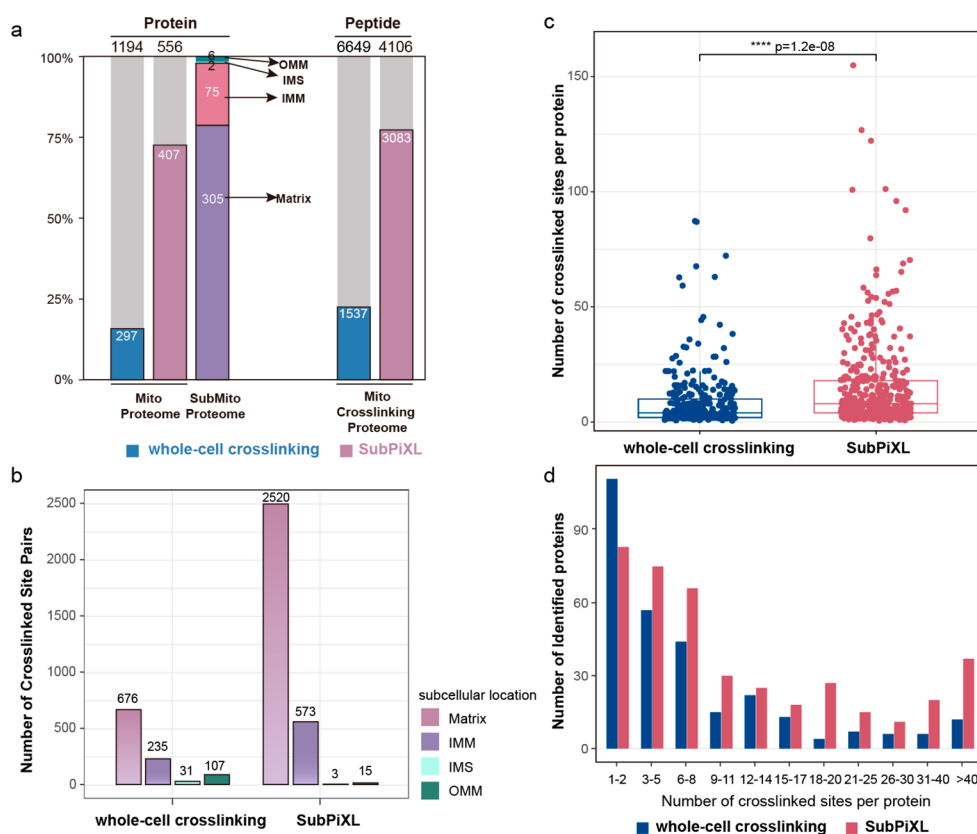


**Figure 2.** Cross-linking identification specificity and coverage of the subcellular proteome. (a) Specificity analysis for the proteome localization of cross-linked proteins and site pairs by the whole-cell cross-linking and SubPiXL, respectively. (b) Refined luminal localization analysis of mitochondria for the cross-linked site pairs. The differential analysis (c) and distribution (d) for the number of cross-linked sites matched to each protein.

capacity of DSDHD. As a result, more cross-linked peptides were identified by DSDHD over BSP in a single LC-MS run and without any enrichment procedure (Table S5). This indicates that DSDHD has suitable membrane permeability and cross-linking reactivity, while the longer spacer arm can enhance the possible benefits of systematic analysis for protein interactions (11.4 Å of BSP vs 16.0 Å of DSDHD).

Next, immunofluorescence imaging was used to identify the correct localization of the protein biotinylation of SubPiXL. Compared with the APEX labeling, the SubPiXL signal showed a consistent spatial location after APEX and subsequent cross-linking treatment (Figure 1b). This indicates no significant change in membrane permeability, ensuring highly selective biotin–phenol labeling with a low off-target before cell lysis. Moreover, the cell viability of SubPiXL treatment was assessed by the CCK-8 analysis. After labeling suborganelle proteins and cellular cross-linking, cell viabilities of 92% and 86% were, respectively, detected, indicating the fitness of SubPiXL for protein conformation and interactions captured in living cells (Figure 1c).

In the case of mitochondrial matrix-targeted SubPiXL, 4106 cross-linked site pairs involved in 556 proteins were identified (Tables S6, S7, and S8). To elucidate the significance of SubPiXL for the suborganelle-targeted protein complex analysis with high specificity and coverage, we compared it in detail with the widely used whole-cell cross-linking (Table S9). Overall, 73% of the 556 proteins were located in mitochondria by SubPiXL, which were much higher than the whole-cell cross-linking results (25% of 1194 proteins). Although our cross-linked mitochondrial proteins have a lower abundance than

whole-cell cross-linking, additional developments are needed to further improve the sensitivity to enhance the XLMS coverage of the mitochondrial proteome (Figure S4). To further study their subcellular location, 98% of 390 proteins with known submitochondrial annotation were located in the matrix and accessible in the inner membrane of mitochondria (IMM). Of the 4106 cross-linked site pairs of the 556 identified proteins, 75% could be mapped to the structural architecture of the mitochondrial proteins. In comparison, only 23% (1537 pairs) of whole-cell cross-linking data were available with a mitochondria location (Figure 2a). As for the submitochondria location, a 3.4-fold increase of cross-linked sites annotated to the matrix and IMM was observed compared to those by whole-cell cross-linking (Figure 2b).

Next, we examined the coverage of the SubPiXL data set by comparing it with the existing proximity labeling data set of the mitochondrial matrix. As Figure S5 shows, 66% of the 556 proteins have been covered by the other two works. As for the remaining 189 proteins, 75 could be mapped to mitochondrial annotation or interact with proteins located in the mitochondria. Biological analysis demonstrated that the other 112 proteins were highly related to mtDNA transcriptional and translation. This indicates that, in addition to proteins located in the mitochondrial matrix, proteins with direct interactions, including transient/weakly interacting proteins, can also be captured by SubPiXL, which enables region-restricted protein complex conformation and interaction interface analysis. As for the reliability of identified cross-links, we examined the number of cross-linked sites on each identified mitochondrial protein. SubPiXL can capture many more cross-linked sites than can be

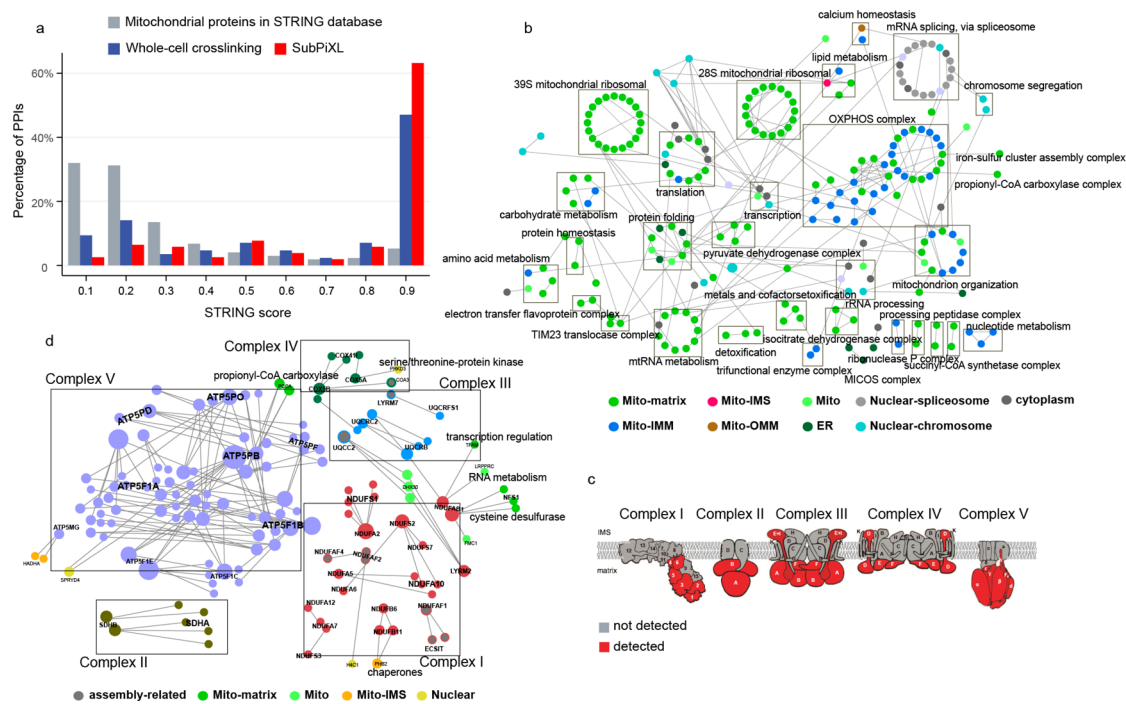


**Figure 3.** SubPiXL based mitochondrial interactome analysis. (a) Evaluation of the PPI confidence for SubPiXL (red), compared to the confidence distribution of PPIs from the human mitochondrial deposit database (gray) and whole-cell cross-linking data set (blue); all the scores were retrieved from the STRING database. (b) Subcellular specific interactome network of all identified PPIs. Nodes represent individual proteins with the annotation of subcellular location according to the UniProt database. (c) Analysis of specificity for cross-linking identification specificity of OXPHOS (complexes I–V). Subunits detected by SubPiXL are shaded red; those not detected are shaded gray. (d) Cross-links within or between the OXPHOS (complexes I–V). The size of the individual nodes indicated the cross-linking density of this residue.

mapped by whole-cell cross-linking (Figure 2c) and has a clear advantage in terms of high matching numbers (Figure 2d), enabling a better protein conformation and interaction analysis with high confidence.

To further investigate the performance of SubPiXL, a detailed comparison was made by referring to the recently published work by Ryl et al.<sup>19</sup> (Table S10). The isolated human mitochondria for XLMS analysis was performed with DSS as a cross-linker. Focused on the identified gene-coding proteins located in the mitochondrial matrix and accessible IMM, 4505 intralinks for 442 proteins as well as 105 PPIs of 112 proteins were obtained using a 275 h LC-MS acquisition. In contrast, 2816 intralinks for 380 proteins and 174 PPIs of 209 proteins were obtained in a 24 h LC-MS acquisition using SubPiXL (Figure S6a). Notably, an obvious abundance difference was observed, in which many more low-abundance intra- and inter-linked mitochondrial proteins were observed in the SubPiXL data, accordingly contributing to higher coverage for PPI identification (Figure S6b). Exclusively identified PPI-related proteins by SubPiXL were highly enriched in biological processes of mitochondrial translation, complex assembly, mRNA splicing, and electron transport (Figure S7). Taken together, all these results demonstrated that high subcellular specificity and identification coverage were achieved by SubPiXL to provide the structural sites for protein complex delineation in the living cells.

**Profiling of Protein Interactomes in the Mitochondrial Matrix.** With the integration of protein isoforms of alternative splicing, 1616 cross-linking sites corresponding to 605 PPIs within 410 proteins were obtained using the SubPiXL strategy. With further insight into their validity, 85.2% of our identified PPIs scored above 0.4% and 63.2% scored above 0.9 (Figure 3a).

The SubPiXL results are more accurate than those from whole-cell cross-linking. This could be attributed to achieving higher coverage for cross-linking identification by targeting suborganelle complexes, enabling an average of 7.19 cross-linked sites for each protein and 5.14 for whole-cell cross-linking. The resulting interaction network was depicted on the basis of highly accurate PPI identification (Figure 3b). In our network, the key functional mitochondrial protein complexes, such as 28S and 39S mitoribosome, the calcium uniporter complex for inward rectification of the  $\text{Ca}^{2+}$  channel, TCA cycle for NADH production, TOM/TIM/PAM protein-import pathway, and the electron-transport chain were all covered. Besides, we found that the majority of the nonmitochondrial localized proteins in our identified network are associated with protein transcription, translation, mRNA splicing, chromatin condensation, and other protein synthesis pathways. We could not rule out the possible existence of these identified proteins in mitochondria. As reported, the mitochondria have an independent genetic material (mtDNA) encoding the mitochondrial rRNAs and tRNAs. While it is unclear how proteins regulate gene expression and the corresponding biosynthetic processes,<sup>20</sup> our results might contribute to the investigation of the mitochondria gene system regulation.

Furthermore, we focused on the significantly attractive protein complex of the oxidative phosphorylation system (OXPHOS), a crucial player of mitochondria in the generation and regulation of cellular bioenergetics to produce the majority of adenosine triphosphate (ATP) molecules.<sup>21</sup> It requires a coordinated transfer of electrons through four multisubunit enzymes (complexes I to IV) that generate a proton gradient across the IMM, while the electrochemical gradient is used by complex V (ATP synthase) to produce ATP. In the topology,

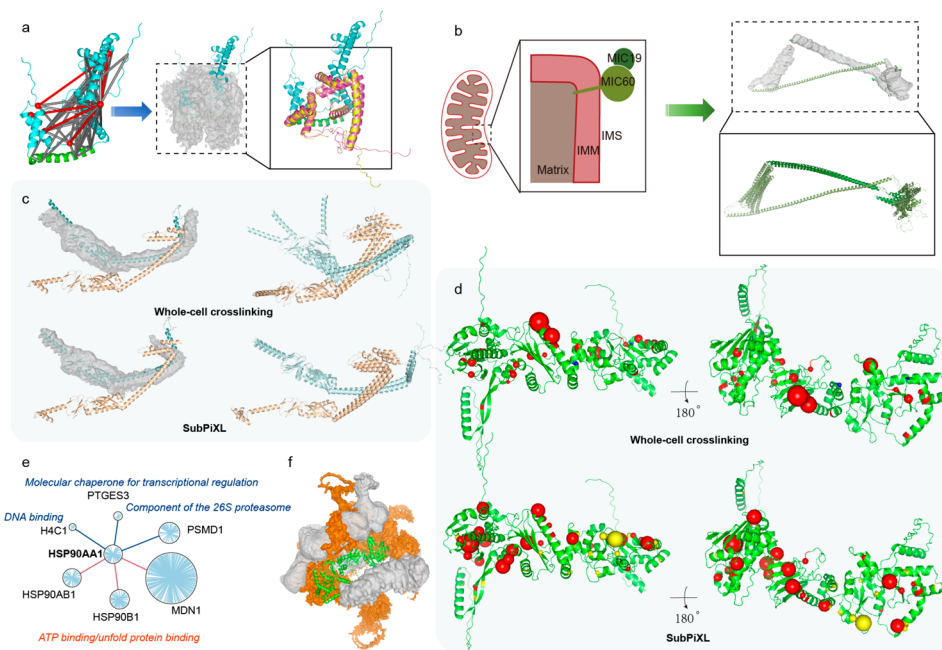


**Figure 4.** Deciphering the specific conformation and interaction of proteins located in the mitochondrial matrix. The protein structural models are all derived from the AlphaFold Protein Structure Database. (a) The dynamic conformation characterization for TFAM. Left: all identified intralinks were mapped onto the protein structure (UniProt accession: Q00059). Cross-links that satisfied (gray) and exceeded (red) the maximum cross-linker distance constraint were shown separately. Right: Ensemble structures that are obtained through joint refinement against XLMS restraints. (b) The structural docking for the MIC60–MIC19 complex. Left: The cellular location of MIC60 and MIC19 in the IMM. Right: Ensemble refinement for the conformation of MIC60–MIC19 with the respective structure (UniProt accession: Q16891 and Q9NX63). (c) Structural models for the protein complex of the PHB complex (P35232 and Q99623) from the refinement against the XLMS restraints, respectively. The top three conformations ranked by energy minimization were shown. (d) Surface distribution of the identified cross-linked sites of HSP90AA1 (P07900). Sites commonly identified by the two strategies are shown in red and exclusively identified, shown in blue (whole-cell cross-linking) and yellow (SubPiXL), respectively. (e) Interaction partner of HSP90AA1. The interactors commonly identified are shown in red, while those exclusively identified by whole-cell cross-linking were shown in blue. (f) Ensemble structures for the protein complex of HSP90AB1 (UniProt accession: P08238) binding with HSP90AA1 by the refinement against the XLMS restraints from whole-cell cross-linking (orange) and SubPiXL (gray) based on the protein structures.

the complexes I–V of OXPHOS are embedded in the IMM connected to the matrix and intermembrane space. Mapped with our SubPiXL data set, only those subunits of OXPHOS with exposure to the matrix space were identified, indicating the high spatial targeting of our strategy (Figure 3c). We also generated an extended OXPHOS subnetwork on the basis of the connectivity of its directly interacting proteins (Figure 3d). In addition to the linkages between the core subunits of OXPHOS (complexes I–V) deposited in the reported structures, some proteins that could be assembly factors docked on the complexes before they matured were also captured, and the corresponding interface sites of these transient interactions were presented. For example, ECSIT, a signal intermediate in the Toll pathway, interacts with the assembly factor NDUFAF1 for the early stage of the complex I; the assembly factor LYRM7 was required for the UQCRCF1 incorporation into the complex III. Biological interactions without structural interfaces were reportedly covered in our data set, such as HADHA assisting mitochondrial respiratory chain complexes during ATP generation, which interacts with ATP5MG in complex V. FMC1 reportedly participates in ATP synthase assembly and interacts with NDUFAF1, which transfers electrons from NADH to the respiratory chain. This demonstrates that suborganelle targeting of SubPiXL facilitates in-depth interaction analysis, further elucidating its function and regulation mechanism.

**Depiction of Structural Architecture for Protein Complexes in the Mitochondrial Matrix.** To illustrate the coverage and validity of identified cross-links for protein

conformation, we first mapped identified K–K linkages onto available high-resolution structures of functional protein complexes in the mitochondrial matrix. First, two important chaperonins with relatively high abundance were analyzed. HSPD1 (573 amino acids with 179 lysines) and HSPE1 (38 amino acids with 11 lysines) facilitate the correct folding of imported proteins in the mitochondrial matrix.<sup>22</sup> Compared to the whole-cell cross-linking, more K–K linkages were captured for HSPD1, whereas no obvious distinction was observed for HSPE1 (Figure S8), while for the spectra matched for these linkages, a 4.7-fold increase for HSPD1 (2054 by SubPiXL vs 432 by whole-cell cross-linking) and 4.3-fold increase for HSPE1 (745 by SubPiXL vs 172 by whole-cell cross-linking) were obtained. Besides, structural compatibility was gained with 95% for HSPD1 and 83% for HSPE1 with reasonable dynamics, in which 31 of the 33 pairs of unmatched linkages fell in the disordered regions. Next, the key functionalized protein complexes located in the mitochondrial matrix were analyzed. The tricarboxylic acid (TCA) cycle and electron transport chain (ETC) are two crucial stages of aerobic respiration. Typically, 55 and 33 cross-links were successfully mapped on the isocitrate dehydrogenase complex (IDH3), which catalyzes the oxidative decarboxylation of isocitrate in the TCA cycle<sup>23</sup> and electron transfer flavoprotein (ETF) complex, which acts as an electron acceptor in the ETC system,<sup>24</sup> with 9% and 100% of cross-links satisfying the distance restraints in the resolved structure, respectively (Figure S9a,b). In addition, for the 28S and 39S mitochondrial ribosomes in the matrix, which encode 13

proteins involved in ETC and OXPHOS, 93% (62 out of 67) and 98% (51 out of 52) of cross-links  $<35$  Å were mapped with high structural compatibility (Figures S9c,d). In addition to the above SLD values, the more stringent SASD-type distance constraints taking into account the protein local topography were determined and further confirmed the validity of the identified cross-links (Figure S9). Moreover, compared to whole-cell cross-linking, SubPiXL allows one to observe a very clear advantage in the number of cross-link identifications for these mitochondrial functional complexes. As a result, more additional linkages with higher confidence could be determined by SubPiXL, which provided a higher capacity for structure delineation of mitochondrial matrix proteins.

As such, the complexes I–V of OXPHOS were illustrated, and the consistency of the resolved crystal structure was checked with our captured cross-links from living cells. In PDB, complexes I, III, and IV have a resolved human structure, while complexes II and V only have structures of porcine and bovine origin. We first mapped the human complex I by identifying cross-links; only K29–K54 in NDUFV1 and K24–K54 in NDUFB6 had  $C\alpha$ – $C\alpha$  distances  $>35$  Å (39.9 and 42.0 Å, respectively; Figure S10a). This is reasonable because these two site pairs fell in the flexible loop region of the protein. When the human structure of complexes III and IV was analyzed, all observed cross-links were within the maximal distance constraint (Figure S10b,c). We then assessed the complexes without a human structure. All 25 cross-links of the porcine complex II structure were satisfied with the distance restraint (Figure S11a). As for the ATP synthase, 45 intersubunit and 97 intrasubunit cross-links were mapped onto the structure of bovine ATP synthase with three states of the ATP production cycle (Figure S11b–d). Almost all cross-links produced a satisfactory distance restraint ( $C\alpha$ – $C\alpha$   $< 35$  Å) among three structures, except for the pair of the K124–K350 on ATP5F1B, which may be due to minor differences between two diverse species or protein states. Taken together, these results demonstrated the suitable performance of SubPiXL to reveal the structural architecture of protein complexes under their cellular environment and further refine the region-restricted structure in the mitochondrial matrix.

**Deciphering Suborganelle-Specific Protein Conformation and Interactions.** On the basis of the successful in situ targeted analysis of protein complexes in the mitochondrial matrix, the dynamic and region-specific structures of protein complexes, especially those with low abundance, were explored to finely outline their structure. TFAM is a transcription factor that plays an important role in initiating and regulating the transcription of mitochondrial DNA.<sup>25</sup> In our data set, 58 intralinks of TFAM were identified, while 5 linkages exceeded 35 Å. The ensemble structures of TFAM were constructed by XLMS restraints to assess its dynamic structure (Figure 4a). One difference was observed between the AF2 and refined structure, suggesting that potential conformation for the presence of TFAM exists in the native microenvironment. Many proteins also reportedly interact by biological validation, but structural evidence is still lacking. For example, CHCHD3 (MIC19) coupled with MIC60 was recognized as the core component of the mitochondrial contact site cristae organizing system (MICOS)<sup>26</sup> and helps generate mitochondrial architecture, lipid metabolism, and protein import. With refinement by 44 intralinks and 3 interlinks in our data set, protein complex docking was achieved via Xplor-NIH (Figure 4b). The conformation of the interacting structure was acquired to

provide the structural blueprint for the study of its biological function.

More than half of the subcellular proteins are multilocalizing proteins. Spatial conformations of protein complexes are close to their functions.<sup>27</sup> The superior spatial resolution of SubPiXL helped us decipher the mitochondria-restricted structure state in living cells, distinguishing them from structures in other subcellular regions. This was exemplified by the PHB complex (PHB–PHB2), which is involved in signaling at the plasma membrane, transcriptional regulation in the nucleus, and homeostasis and signal transduction in the mitochondrion.<sup>28</sup> To clarify its specific conformation over mitochondria, the ensemble structure of the PHB complex was performed by refinement against the data set by SubPiXL and whole-cell cross-linking. A distinction was presented between these two structures with more convergent structural conformation using SubPiXL data (Figure 4c). Moreover, we moved to illustrate how region-restricted conformation drives diverse interactions. Heat shock protein 90 (HSP90) belongs to the family of molecular chaperones and is essential for maintaining intracellular protein homeostasis, which has been widely applied for targeted proteins to inhibit signaling pathways in tumor cells.<sup>29</sup> However, it is difficult to confirm its target proteins due to their highly flexible structure and wide distribution in cells. HSP90AA1 is one of the most important components of the HSP90 family with multiple localizations and is reportedly involved in tumor progression and cancer cell invasion. We first determined the solvent accessibility of the HSP90AA1 surface by delineating the distribution of the identified cross-linked sites to display the exposed state of the protein surface and compared it with the whole-cell state. The distributions of available sites on the protein surface differed significantly (Figure 4d). Specifically, the region among the amino acid sequences of 58–152 and 477–546 showed a relatively low labeling capability in mitochondria; the sequence of 407–443 is inversely dominated. Interactor analysis was explored to assess protein functions and dynamics in the context of a cell (Figure 4e). Proteins of HSP90AB1, HSP90B1, and MDN1 involved in ATP or unfold protein binding were found as interactors of HSP90AA1 in both results, while additional functions, such as the components of 26S proteasome, were exclusively identified from whole-cell cross-linking. Among the commonly identified interactions, HSP90AA1 and HSP90AB1 have highly identical amino acid sequences and are differentially regulated physiologically and under heat shock.<sup>30</sup> To decipher the differences in heterodimer conformation, they form in mitochondria differently from that in the whole cell, and the ensemble structure was constructed by refinement against the identified cross-links. Several domains in the two conformations overlap, but most are unique (Figure 4f). As such, specific conformations might exist in mitochondria, signifying the diversity of biological functions, and these conformations need to be further evaluated and cross-validated by other experimental methods such as NMR and Cryo-EM. These results demonstrate the ability of SubPiXL to clarify the dynamics and region-restricted conformations for protein complexes with suborganelle resolution, contributing to their functional understanding.

## CONCLUSIONS

The dissection of the protein complexes at a high spatial resolution is important for the identification of the region-restraint components and conformation needed for functional clarification. In this study, we developed a SubPiXL (sub-

organelle proteome labeling assisted in vivo cross-linking) strategy to decipher the protein complex assembly at a high spatial resolution. Similar to in vivo XLMS and PL, SubPiXL can fix the protein conformational state of living cells and overcomes the major limitation of in vivo cross-linking, which is incapable of displaying the structural architecture at a high spatial resolution. Using APEX-mito-expressing HEK293T cells as a proof-of-concept system, we demonstrated that 76% PPIs identified by the SubPiXL approach were mapped to the mitochondrial matrix and accessible IMM. Compared to previous studies that applied organelle isolation before chemical cross-linking, this allowed for refined spatial characterization of the subcompartment of the cellular organelle, which allowed for the capture of more PPIs with high dynamics. Furthermore, the high spatial resolution and identification coverage of SubPiXL in XLMS analysis provided the suborganelle-targeted structural dynamics and interactional interface docking for protein complexes, and for the multilocalized proteins, the specific conformation and interactions in a certain region could be clarified and distinguished from that in other compartments. Moreover, just as demonstrated in the mitochondrial matrix, SubPiXL is suitable for all the other membrane-bound suborganelles, such as the nucleus and ER lumen, as well as for those of “open” regions without membrane enclosures, such as the OMM and ER membrane. Therefore, the SubPiXL strategy is a promising tool for the exploration of the region-restricted structures and functional consequences of protein complexes in various suborganelles.

## ■ ASSOCIATED CONTENT

### SI Supporting Information

The Supporting Information is available free of charge at <https://pubs.acs.org/doi/10.1021/acs.analchem.2c01637>.

Experimental details, DSDHD characterization (Figures S1–S3, Table S5), specificity and coverage characterization of SubPiXL (Table S9, Figures S4 and S5), comparison of the identified proteins by isolated mitochondria cross-linking and SubPiXL (Figures S6 and S7), and validation of the structural architecture for the protein complex in the mitochondrial matrix (Figures S8–S11) (PDF)

Isolated identified cross-links for TFAM (Table S1), MIC60 and MIC19 (Table S2), PHB and PHB2 (Table S3), and HSP90AA1 and HSP90AB1 (Table S4), identified cross-links and protein subcellular annotation by SubPiXL (Tables S6 and S8), identified cross-linking sites by whole-cell cross-linking (Table S7), list of intra- and inter-protein links by SubPiXL and isolated mitochondria cross-linking (Table S10), and list of the protein full name with the corresponding gene name (Table S11) (XLSX)

## ■ AUTHOR INFORMATION

### Corresponding Authors

**Qun Zhao** – CAS Key Laboratory of Separation Science for Analytical Chemistry, National Chromatographic R. & A. Center, Dalian Institute of Chemical Physics, Chinese Academy of Science, Dalian, Liaoning 116023, China; University of Chinese Academy of Sciences, Beijing 100039, China; Phone: +86-411-84379720; Email: [zhaoqun@dicp.ac.cn](mailto:zhaoqun@dicp.ac.cn)

**Lihua Zhang** – CAS Key Laboratory of Separation Science for Analytical Chemistry, National Chromatographic R. & A.

Center, Dalian Institute of Chemical Physics, Chinese Academy of Science, Dalian, Liaoning 116023, China; University of Chinese Academy of Sciences, Beijing 100039, China; [orcid.org/0000-0002-8260-7951](https://orcid.org/0000-0002-8260-7951); Phone: +86-411-84379720; Email: [lihuazhang@dicp.ac.cn](mailto:lihuazhang@dicp.ac.cn)

### Authors

**Yuxin An** – CAS Key Laboratory of Separation Science for Analytical Chemistry, National Chromatographic R. & A. Center, Dalian Institute of Chemical Physics, Chinese Academy of Science, Dalian, Liaoning 116023, China; University of Chinese Academy of Sciences, Beijing 100039, China

**Zhou Gong** – Innovation Academy for Precision Measurement Science and Technology, Chinese Academy of Sciences, Wuhan 430071, China

**Lili Zhao** – CAS Key Laboratory of Separation Science for Analytical Chemistry, National Chromatographic R. & A. Center, Dalian Institute of Chemical Physics, Chinese Academy of Science, Dalian, Liaoning 116023, China; University of Chinese Academy of Sciences, Beijing 100039, China

**Yi Li** – College of Chemistry and Molecular Engineering, Synthetic and Functional Biomolecules Center, Beijing National Laboratory for Molecular Sciences, Key Laboratory of Bioorganic Chemistry and Molecular Engineering of Ministry of Education, Peking University, Beijing 100871, China

**Zhen Liang** – CAS Key Laboratory of Separation Science for Analytical Chemistry, National Chromatographic R. & A. Center, Dalian Institute of Chemical Physics, Chinese Academy of Science, Dalian, Liaoning 116023, China; University of Chinese Academy of Sciences, Beijing 100039, China

**Peng Zou** – College of Chemistry and Molecular Engineering, Synthetic and Functional Biomolecules Center, Beijing National Laboratory for Molecular Sciences, Key Laboratory of Bioorganic Chemistry and Molecular Engineering of Ministry of Education and Peking-Tsinghua Center for Life Sciences, PKU-IDG/McGovern Institute for Brain Research, Peking University, Beijing 100871, China; [orcid.org/0000-0002-9798-5242](https://orcid.org/0000-0002-9798-5242)

**Yukui Zhang** – CAS Key Laboratory of Separation Science for Analytical Chemistry, National Chromatographic R. & A. Center, Dalian Institute of Chemical Physics, Chinese Academy of Science, Dalian, Liaoning 116023, China; University of Chinese Academy of Sciences, Beijing 100039, China

Complete contact information is available at:

<https://pubs.acs.org/10.1021/acs.analchem.2c01637>

### Notes

The authors declare no competing financial interest.

## ■ ACKNOWLEDGMENTS

This work was supported by the National Natural Science Foundation of China (32088101, 22074139, 21991083, 21725506, 21727806), National Key R&D Program of China (2018YFA0507703, 2020YFE0202200, 2021YFA1301501), the Ministry of Science and Technology (2018YFA0507600, 2017YFA0503600), and the Youth Innovation Promotion Association, CAS (2020184). P.Z. is sponsored by a Bayer Investigator Award.

## ■ REFERENCES

- Scott, J. D.; Pawson, T. *Science* **2009**, 326, 1220–1224.
- Guin, D.; Gruebele, M. *Chem. Rev.* **2019**, 119, 10691–10717.

- (3) Zhu, H.; Tamura, T.; Hamachi, I. *Curr. Opin. Chem. Biol.* **2019**, *48*, 1–7.
- (4) Huttlin, E. L.; Bruckner, R. J.; Paulo, J. A.; Cannon, J. R.; Ting, L.; Baltier, K.; Colby, G.; Gebreab, F.; Gygi, M. P.; Parzen, H.; Szpyt, J.; Tam, S.; Zarraga, G.; Pontano-Vaites, L.; Swarup, S.; White, A. E.; Schweppe, D. K.; Rad, R.; Erickson, B. K.; Obar, R. A.; Guruharsha, K. G.; Li, K.; Artavanis-Tsakonas, S.; Gygi, S. P.; Harper, J. W. *Nature* **2017**, *545*, 505–509.
- (5) Kristensen, A. R.; Gsponer, J.; Foster, L. J. *Nat. Methods* **2012**, *9*, 907–909.
- (6) Zheng, Y.; Zhang, C.; Croucher, D. R.; Soliman, M. A.; St-Denis, N.; Pasculescu, A.; Taylor, L.; Tate, S. A.; Hardy, W. R.; Colwill, K.; Dai, A. Y.; Bagshaw, R.; Dennis, J. W.; Gingras, A. C.; Daly, R. J.; Pawson, T. *Nature* **2013**, *499*, 166–171.
- (7) Iacobucci, C.; Gotze, M.; Sinz, A. *Curr. Opin. Biotechnol.* **2020**, *63*, 48–53.
- (8) Wheat, A.; Yu, C.; Wang, X.; Burke, A. M.; Chemmama, I. E.; Kaake, R. M.; Baker, P.; Rychnovsky, S. D.; Yang, J.; Huang, L. *Proc. Natl. Acad. Sci. U. S. A.* **2021**, *118*, e2023360118.
- (9) Chavez, J. D.; Lee, C. F.; Caudal, A.; Keller, A.; Tian, R.; Bruce, J. E. *Cell Syst* **2018**, *6*, 136–141.e5.
- (10) Lundberg, E.; Borner, G. H. H. *Nat. Rev. Mol. Cell Biol.* **2019**, *20*, 285–302.
- (11) Zhou, Y.; Zou, P. *Curr. Opin. Chem. Biol.* **2021**, *60*, 30–38.
- (12) Li, Y.; Tian, C.; Liu, K.; Zhou, Y.; Yang, J.; Zou, P. *Cell. Chem. Biol.* **2020**, *27*, 858–865.
- (13) Go, C. D.; Knight, J. D. R.; Rajasekharan, A.; Rathod, B.; Hesketh, G. G.; Abe, K. T.; Youn, J. Y.; Samavarchi-Tehrani, P.; Zhang, H.; Zhu, L. Y.; Popiel, E.; Lambert, J. P.; Coyaud, E.; Cheung, S. W. T.; Rajendran, D.; Wong, C. J.; Antonicka, H.; Pelletier, L.; Palazzo, A. F.; Shoubridge, E. A.; Raught, B.; Gingras, A. C. *Nature* **2021**, *595*, 120–124.
- (14) Zhou, Y.; Wang, G.; Wang, P.; Li, Z.; Yue, T.; Wang, J.; Zou, P. *Angew. Chem., Int. Ed. Engl.* **2019**, *58*, 11763–11767.
- (15) Merkle, E. D.; Rysavy, S.; Kahraman, A.; Hafen, R. P.; Daggett, V.; Adkins, J. N. *Protein Sci.* **2014**, *23*, 747–759.
- (16) Ferrari, A. J. R.; Clasen, M. A.; Kurt, L.; Carvalho, P. C.; Gozzo, F. C.; Martinez, L. *Bioinformatics* **2019**, *35*, 3169–3170.
- (17) An, Y.; Zhao, Q.; Gao, H.; Zhao, L.; Li, X.; Zhang, X.; Liang, Z.; Zhang, L.; Zhang, Y. *Anal. Chem.* **2022**, *94*, 3904–3913.
- (18) Gao, H.; Zhao, L.; Zhong, B.; Zhang, B.; Gong, Z.; Zhao, B.; Liu, Y.; Zhao, Q.; Zhang, L.; Zhang, Y. *Anal. Chem.* **2022**, *94*, 7551–7558.
- (19) Ryl, P. S. J.; Bohlke-Schneider, M.; Lenz, S.; Fischer, L.; Budzinski, L.; Stuver, M.; Mendes, M. M. L.; Sinn, L.; O'Reilly, F. J.; Rappsilber, J. *J. Proteome Res.* **2020**, *19*, 327–336.
- (20) Greber, B. J.; Ban, N. *Annu. Rev. Biochem.* **2016**, *85*, 103–132.
- (21) Bergman, O.; Ben-Shachar, D. *Can. J. Psychiatry* **2016**, *61*, 457–469.
- (22) Levy-Rimler, G.; Viitanen, P.; Weiss, C.; Sharkia, R.; Greenberg, A.; Niv, A.; Lustig, A.; Delarea, Y.; Azem, A. *Eur. J. Biochem.* **2001**, *268*, 3465–3472.
- (23) Sun, P.; Ma, T.; Zhang, T.; Zhu, H.; Zhang, J.; Liu, Y.; Ding, J. J. *Biol. Chem.* **2019**, *294*, 16214–16227.
- (24) Henriques, B. J.; Katrine Jentoft Olsen, R.; Gomes, C. M.; Bross, P. *Gene* **2021**, *776*, 145407.
- (25) Ngo, H. B.; Kaiser, J. T.; Chan, D. C. *Nat. Struct. Mol. Biol.* **2011**, *18*, 1290–1296.
- (26) Zerbes, R. M.; Hoss, P.; Pfanner, N.; van der Laan, M.; Bohnert, M. *J. Mol. Biol.* **2016**, *428*, 1485–1492.
- (27) Yang, L.; Lv, Y.; Li, T.; Zuo, Y.; Jiang, W. J. *Theor. Biol.* **2014**, *358*, 61–73.
- (28) Yoshinaka, T.; Kosako, H.; Yoshizumi, T.; Furukawa, R.; Hirano, Y.; Kuge, O.; Tamada, T.; Koshiba, T. *iScience* **2019**, *19*, 1065–1078.
- (29) Stauffer, K.; Stoeltzing, O. *Curr. Cancer Drug Targets* **2010**, *10*, 890–897.
- (30) Cheng, M. B.; Zhang, Y.; Zhong, X.; Sutter, B.; Cao, C. Y.; Chen, X. S.; Cheng, X. K.; Zhang, Y.; Xiao, L.; Shen, Y. F. *Cell. Signal.* **2010**, *22*, 1206–1213.

## Recommended by ACS

### Quantitative Structural Proteomics Unveils the Conformational Changes of Proteins under the Endoplasmic Reticulum Stress

Kejun Yin, Ronghu Wu, *et al.*

SEPTEMBER 15, 2022  
ANALYTICAL CHEMISTRY

READ 

### Monitoring Protein Import into the Endoplasmic Reticulum in Living Cells with Proximity Labeling

Ziqi Lyu, Joseph C. Genereux, *et al.*

JUNE 08, 2022  
ACS CHEMICAL BIOLOGY

READ 

### Deep Single-Cell-Type Proteome Profiling of Mouse Brain by Nonsurgical AAV-Mediated Proximity Labeling

Xiaojun Sun, Junmin Peng, *et al.*

MARCH 22, 2022  
ANALYTICAL CHEMISTRY

READ 

### In-Depth *In Vivo* Crosslinking in Minutes by a Compact, Membrane-Permeable, and Alkynyl-Enrichable Crosslinker

Hang Gao, Yukui Zhang, *et al.*

MAY 16, 2022  
ANALYTICAL CHEMISTRY

READ 

Get More Suggestions >